ACS OMEGA

http://pubs.acs.org/journal/acsodf

Article

Theoretical Investigation of Spectroscopic Properties of the Alkaline-Earth-Metal Monohydrides toward Laser Cooling and Magneto-Optical Trapping

Renjun Pang, Junhao Yin, Yueyang Wang, Qinning Lin, Zesen Wang, Liang Xu, Shunyong Hou, Hailing Wang, Jianping Yin,* and Tao Yang*

Cite This: *ACS Omega* 2023, 8, 19391−19401

Read Online

ACCESS | Metrics & More | Article Recommendations

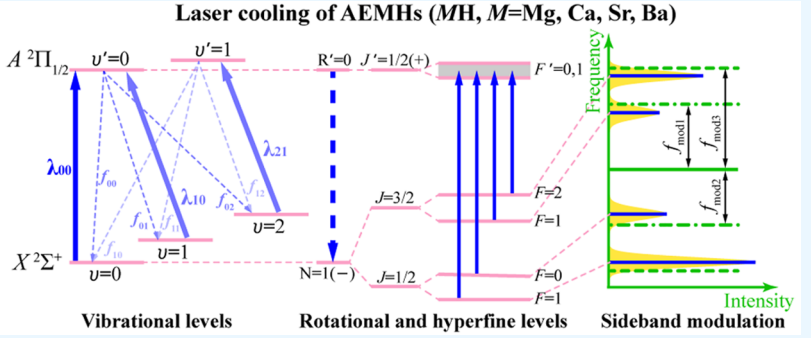

ABSTRACT: Alkaline-earth-metal monohydrides *M*H (*M* = Be, Mg, Ca, Sr, Ba) have long been regarded as promising candidates toward laser cooling and trapping; however, their rich internal level structures that are amenable to magneto-optical trapping have not been completely explored. Here, we first systematically evaluated Franck−Condon factors of these alkaline-earth-metal monohydrides in the $A^2\Pi_{1/2} \leftarrow X^2\Sigma^+$ transition, exploiting three respective methods (the Morse potential, the closed-form approximation, and the Rydberg−Klein−Rees method). The effective Hamiltonian matrix was introduced for MgH, CaH, SrH, and BaH individually in order to figure out their molecular hyperfine structures of $X^2\Sigma^+$, the transition wavelengths in the vacuum, and hyperfine branching ratios of $A^2\Pi_{1/2}(J' = 1/2,+) \leftarrow X^2\Sigma^+(N = 1,-)$, followed by possible sideband modulation proposals to address all hyperfine manifolds. Lastly, the Zeeman energy level structures and associated magnetic *g* factors of the ground state $X^2\Sigma^+(N = 1,-)$ were also presented. Our theoretical results here not only shed more light on the molecular spectroscopy of alkaline-earth-metal monohydrides toward laser cooling and magneto-optical trapping but also can contribute to research in molecular collisions involving few-atom molecular systems, spectral analysis in astrophysics and astrochemistry, and even precision measurement of fundamental constants such as the quest for nonzero detection of electron's electric dipole moment.

INTRODUCTION

Compared with atoms, diatomic molecules have a sophisticated energy level structure that on one side can directly bring more challenges to the manipulation and control of them, such as laser cooling and magneto-optical trapping, and on the other side exhibit enhanced sensitivity in precision measurement such as the searches for fundamental symmetry violations, as well as broadening the horizon of molecular reaction dynamics of cold molecules and their astrophysical relevance.[1−9] As early as 2004, Di Rosa presented a brief survey of candidate molecules for laser cooling and magneto-optical trapping,[10] after which polar heavy-atom molecules SrF,[11,12] CaF,[13,14] and YO[15,16] have already been successfully demonstrated in direct laser cooling techniques and magneto-optical traps (MOTs). DeMille and his co-workers first demonstrated the optical cooling cycle for SrF in the $A^2\Pi_{1/2} \leftarrow X^2\Sigma^+$ transition[17] and further realized its transverse cooling in a substantial flux at velocities <50 m/s,[11,18] prior to its capture in the three-dimensional (3D) MOT at temperatures of 2.5 mK, 250 μK, and 14 μK, respectively.[12,19,20] For CaF, Tarbutt and co-workers were able to achieve a cooling temperature of 50 μK in a 3D optical molasses, which is well below the Doppler limit.[21] Doyle's group, on the contrary, obtained a relatively higher cooling temperature of 340 μK for CaF in a radio-frequency

Received: January 17, 2023
Accepted: April 10, 2023
Published: May 24, 2023

Table 1. Spectroscopic Constants Adopted in Calculating Franck−Condon Factors of MH (M = Be, Mg, Ca, Sr, and Ba) in Their $A^2\Pi_{1/2} \leftarrow X^2\Sigma^+$ Transition

Molecule	State	T_e (cm^{-1})	ω_e (cm^{-1})	$\omega_e\chi_e$ (cm^{-1})	r_e (Å)	τ (ns)
BeH	$X^2\Sigma^+$	0	2060.78[58]	36.31[58]	1.3426[58]	-
	$A^2\Pi_{1/2}$	20033.2[58]	2088.58[58]	40.14[58]	1.3336[58]	81[45−48,50]
MgH	$X^2\Sigma^+$	0	1492.78[59−61]	29.85[59−61]	1.7300[59−61]	-
	$A^2\Pi_{1/2}$	19225.5[59−61]	1600.33[59−61]	31.87[59−61]	1.6780[59−61]	43.6[45−48,50]
CaH	$X^2\Sigma^+$	0	1298.34[58]	19.1[58]	2.0025[58]	-
	$A^2\Pi_{1/2}$	14413.0[58]	1333[58]	20[58]	1.9740[58]	33.2[45−48,50]
SrH	$X^2\Sigma^+$	0	1207.04[36]	17.11[36]	2.1461[36]	-
	$A^2\Pi_{1/2}$	13500.6[36]	1253.91[36]	18.03[36]	2.1209[36]	33.8[45−48,50]
BaH	$X^2\Sigma^+$	0	1168.31[58]	14.50[58]	2.2318[58]	-
	$A^2\Pi_{1/2}$	9457.5[58]	1110.55[58]	15.29[58]	2.2490[58]	136.5[45−48,50]

(RF) MOT, but with a larger number of trapped molecules and a higher density at nearly 1 order of magnitude.[22] Ye's group also reported a 3D RF MOT for the YO molecule at a temperature of 4.1 mK, which is the first MOT of a nonfluoride molecule ever.[23] Other molecular candidates have also been investigated for laser cooling and trapping either theoretically or in a spectroscopic approach, including but not limited to YbF,[24] RaF,[25] BaF,[26] HgF,[27] MgF,[28] and BH,[29] or even SrOH[30,31] and YbOH.[32] It is worth noting that polar heavy-atom fluoride molecules that are laser-coolable, such as YbF, RaF, BaF, or HgF, exhibit certain sensitivities to new physics beyond the standard model such as the measurement of the electron's electric dipole moment (eEDM).[32] However, such a uniqueness requires a strong electric field in the lab (technically higher than 10 kV/cm) to polarize and does not admit an internal comagnetometer, both of which leave them vulnerable to systematic effects in the precision measurement.

Alkaline-earth-metal monohydrides (AEMHs) MH (M = Be, Mg, Ca, Sr and Ba) are widely found in sunspots, stars, nebulae, and the interstellar medium, whose spectral data can provide substantial insight into the astrophysical environments in which they were found. The rovibrational spectra of BeH, MgH, and CaH in their $X^2\Sigma^+$ state as well as MgH and CaH in their $A^2\Pi_{1/2}$ and $B^2\Sigma^+$ states have been well characterized by the spectroscopic models in the ExoMol project.[33,34] Apart from these astronomical efforts, Steimle et al. measured $A^2\Pi_{1/2}(v' = 0,1)/B^2\Sigma^+(v' = 0) - X^2\Sigma^+(v = 0)$ band systems of CaH in laser-induced fluorescence spectroscopy at a resolution of about ±90 MHz.[35] Other $A^2\Pi_{1/2}(v' = 0,1) - X^2\Sigma^+$ ($v = 0$) band systems have also been explored in BeH, MgH, and SrH via either excitation spectroscopy or Fourier transform emission spectroscopy.[36−38] AEMHs such as CaH were also extensively investigated in elastic,[39] inelastic nonreactive,[40] and inelastic reactive[41] collisions, opening up new means of controlling internal states and chemical reactions near cold and ultracold temperature regimes. More importantly, AEMHs are considered competitive candidates for laser cooling and trapping[10,42,43] and may help in probing exotic quantum phases and eEDM due to their large permanent dipole moments.[44]

Previous studies revealed the laser cooling features of AEMHs in the following aspects: (i) highly diagonal Franck−Condon factor (FCF) that describes the overlap of vibrational wave functions involved in the cooling optical transition ($A^2\Pi_{1/2} \leftarrow X^2\Sigma^+$); (ii) short radiative lifetime of the $A^2\Pi_{1/2}$ state (^{9}BeH: 81 ns,[45] ^{24}MgH: 43.6 ns,[46] ^{40}CaH: 33.2 ns,[47] ^{88}SrH: 33.8 ns,[48] and ^{138}BaH: 136.5 ns[49,50]), which corresponds to strong spontaneous radiation decay rate; (iii) no intervening electronic states (except BaH) in the $X^2\Sigma^+ \leftarrow A^2\Pi_{1/2}$ transition. Recently, BaH has been extensively examined by Zelevinsky et al. both theoretically via *ab initio* calculations and experimentally via spectroscopic detection and direct laser cooling.[50−53] They obtained vibrational branching ratios for $B^2\Sigma^+ - X^2\Sigma^+$ and $A^2\Pi_{1/2} - X^2\Sigma^+$ optical cycling transitions using fluorescence and absorption detection, confirming the $A^2\Pi_{1/2}$ state as a superior choice for laser cooling rather than the $B^2\Sigma^+$ state, based on which Zelevinsky et al. adopted $A^2\Pi_{1/2} \leftarrow X^2\Sigma^+$ as the optical cycling transition while repumping excited vibrational levels of the ground state through the $B^2\Sigma^+$ state. Some research groups are also considering CaH[10,54,55] and SrH[56] as candidates for laser cooling. In general, AEMHs have been analyzed theoretically using the *ab initio* quantitative method to build their potential energy curves, vibrational transitions, and FCFs;[33,42,43] however, a systematic spectroscopic evaluation of AEMHs toward laser cooling and magneto-optical trapping is still missing.

In this paper, we first visited the FCFs of AEMHs in the $A^2\Pi_{1/2} \leftarrow X^2\Sigma^+$ transition using the Morse potential method, the closed-form approximation (CFA) method, and the Rydberg−Klein−Rees (RKR) method separately, which agree nicely with previous results that these FCFs are all highly diagonal.[42] The wavelengths proposed for the main cycling laser λ_{00} were calculated to be 498.849 nm (BeH), 518.705 nm (MgH), 692.996 nm (CaH), 739.438 nm (SrH), and 1060.630 nm (BaH), respectively, which are closer to previous experimental values[36,38,50,57,58] than the results in ref 29. Subsequently, we employed the effective Hamiltonian approach to evaluate molecular hyperfine structures in the $X^2\Sigma^+$ state of MgH, CaH, SrH, and BaH in order to implement nearly closed optical transitions. Based on the J mixing nature in the $X^2\Sigma^+(N = 1,-)$ state, we evaluated the hyperfine branching ratios for $A^2\Pi_{1/2}(J' = 1/2,+) \leftarrow X^2\Sigma^+(N = 1,-)$, and proposed suitable sideband modulation schemes to simultaneously cover all hyperfine transitions in each molecule. In the end, we analyzed the Zeeman level structures of the $X^2\Sigma^+(N = 1,-)$ state and associated magnetic g factors with or without J mixing.

RESULTS AND DISCUSSION

Vibrational Transitions and Franck−Condon Factors between $X^2\Sigma^+$ and $A^2\Pi_{1/2}$ States. We first characterized the optical transition schemes between $X^2\Sigma^+$ and $A^2\Pi_{1/2}$ for five AEMHs MH (M = Be, Mg, Ca, Sr, and Ba). For BeH, MgH, CaH, and SrH, there are no intermediate electronic states

https://doi.org/10.1021/acsomega.3c00352
ACS Omega 2023, 8, 19391−19401

Table 2. Computed Franck−Condon Factors of AEMHs by Three Respective Methods (Numbers in Parentheses Indicate the Power of 10)

Molecule	Methods	f_{00}	f_{01}	f_{02}	f_{11}	Ref
BeH	Morse potential	0.9980	0.0018	0.0001	0.9950	This work
	CFA	0.9977	0.0022	<0.0001	0.9932	This work
	RKR	0.9977	0.0022	<0.0001	0.9933	This work
	-	0.998	0.002	3.8(−5)	0.995	Cal.[42]
MgH	Morse potential	0.9420	0.0576	0.0003	0.8340	This work
	CFA	0.9429	0.0553	0.0016	0.8354	This work
	RKR	0.9541	0.0445	0.0013	0.8679	This work
	-	0.954	0.042	0.003	0.870	Cal.[42]
	-	0.94	0.06	-	-	Exp.[69]
CaH	Morse potential	0.9850	0.0146	0.0004	0.9560	This work
	CFA	0.9846	0.0152	0.0001	0.9545	This work
	RKR	0.9954	0.0045	<0.0001	0.9863	This work
	-	0.961	0.038	0.002	0.885	Cal.[42]
	-	0.9572	0.0386	0.0042	-	Exp.[55]
SrH	Morse potential	0.9890	0.0110	<0.0001	0.9660	This work
	CFA	0.9886	0.0113	<0.0001	0.9661	This work
	RKR	0.9995	0.0004	<0.0001	0.9985	This work
	-	0.978	0.021	6.0(−4)	0.935	Cal.[42]
BaH	Morse potential	0.9940	0.0059	0.0001	0.9800	This work
	CFA	0.9950	0.0050	<0.0001	0.9851	This work
	RKR	0.9711	0.0286	<0.0001	0.9151	This work
	-	0.971	0.029	7.0(−5)	0.913	Cal.[42]

between $X^2\Sigma^+$ and $A^2\Pi_{1/2}$; however, the $A^2\Pi_{1/2} - X^2\Sigma^+$ cooling scheme of BaH has a loss channel involving another intermediate state $H^2\Delta_{3/2}$. Note that the Einstein $\mathcal{A}$ coefficients of $A^2\Pi_{1/2}(v' = 0) \rightarrow X^2\Sigma^+ (v = 0)$ and $A^2\Pi_{1/2}(v' = 0) \rightarrow H^2\Delta_{3/2} (v = 0)$ are 7.30×10^6/s and 4.24×10^2/s, respectively, while the decay rate of $A^2\Pi_{1/2} \rightarrow X^2\Sigma^+$ is far more than that of $A^2\Pi_{1/2} \rightarrow H^2\Delta_{3/2}$.[49] Therefore, the unwanted $A^2\Pi_{1/2} \rightarrow H^2\Delta_{3/2}$ leakage is less likely to limit the laser cooling process significantly, and we can choose the transition $A^2\Pi_{1/2} \leftarrow X^2\Sigma^+$ as the major cooling channel of BaH as well.

Highly diagonal FCFs can help determine the vibrational branching ratios and numbers of cooling lasers. The molecular parameters of $X^2\Sigma^+$ and $A^2\Pi_{1/2}$ for AEMHs in our calculations are summarized in Table 1. For the $A^2\Pi_{1/2} \rightarrow X^2\Sigma^+$ transition, we computed FCFs in three different methods, i.e., the Morse potential method,[62] the CFA method,[63] and the RKR method.[64−67] The Morse potential energy function takes the form $V(r) = D_e[(1 - e^{-\alpha(r-r_e)})^2 - 1]$, where r is the distance between the atoms, r_e is the equilibrium bond distance, D_e is the well depth, and α controls the width of the potential. In detail, $D_e = \hbar\omega_e^2/4\omega_e\chi_e$ and $\omega_e\chi_e = \alpha^2\hbar/2\mu$ (the potential is characterized by the depth D_e and the range α; μ, ω_e, and $\omega_e\chi_e$ represent the reduced mass and the standard harmonic and anharmonic spectroscopic parameters, respectively). The CFA method to estimate FCFs for the molecular band systems, as is often the case for astrophysically interesting molecules such as CeO, CrH, CrO, CuH, GeH, LaO, NiH, SnH, and ZnH, is based solely on μ, ω_e, and r_e.[67] In the RKR method, the relevant potential energy curve is obtained by calculating the classical turning points according to the vibrational and rotational constants of the corresponding state of molecules rather than by imposing an analytic form, so the RKR method is more persuasive.[68] Some of the calculated FCFs are compiled in Table 2. Note that in any method, the sum of f_{00}, f_{01}, and f_{02} for each AEMH molecule is greater than 0.9999, indicating that almost 1×10^4 photons can be scattered to slow the molecules with merely three cooling lasers.[2,17] The theoretical results mentioned above are also in good agreement with those in ref 42. In addition, the respective FCFs of MgH and CaH have been determined experimentally,[55,69] indicating that FCFs of MgH are consistent with our calculations. The calculated FCFs of CaH are slightly larger than the experimental values since the measured main cooling and repumping wavelengths are different from earlier experimental values. We calculated the wavelengths of the $A^2\Pi_{1/2} \leftarrow X^2\Sigma^+$ transition as well, which agree nicely with the experimental results as listed in Table 3.

Table 3. Comparison List of Transition Wavelengths for the Three Major Pumping Channels λ_{00}, λ_{10}, and λ_{21} between the $X^2\Sigma^+$ and $A^2\Pi_{1/2}$ States of AEMHs

Molecule	λ_{00} (nm)	λ_{10} (nm)	λ_{21} (nm)	Ref
BeH	498.849	553.772	550.942	This work
	499.2	554.2	-	Exp.[38]
	497.2	551.3	548.3	Cal.[42]
MgH	518.705	560.359	555.281	This work
	518.7	562.3	-	Exp.[58]
	518.7	560.3	-	Exp.[69]
	525.5	568.1	563.6	Cal.[42]
CaH	692.996	759.303	755.229	This work
	693.0	759.3	-	Exp.[57]
	695.13	761.87	-	Exp.[55]
	675.4	738.0	732.0	Cal.[42]
SrH	739.438	809.654	804.492	This work
	739.4	815.0	-	Exp.[36]
	740.3	811.1	805.0	Cal.[42]
BaH	1060.630	1206.410	1210.840	This work
	1060.8	-	-	Exp.[50]
	952.6	1067.7	1070.3	Cal.[42]

https://doi.org/10.1021/acsomega.3c00352
ACS Omega 2023, 8, 19391−19401

Table 4. Spectral Constants of the Ground $X^2\Sigma^+$ State of MgH, CaH, SrH, and BaH

Molecules	B_v (MHz)	D_v (MHz)	γ_v (MHz)	b_v (MHz)	c_v (MHz)
MgH	171976.150[72]	10.612[72]	791.10[72]	306.8[72]	3.15[72]
CaH	126772.935[73]	5.546[73]	1305.755[73]	155.785[73]	4.74[73]
SrH	109003.2[74]	4.06992[74]	3719.73[74]	121[75]	2[75]
BaH	100487.721[76]	3.381171[76]	5761.89[76]	46[75]	1[75]

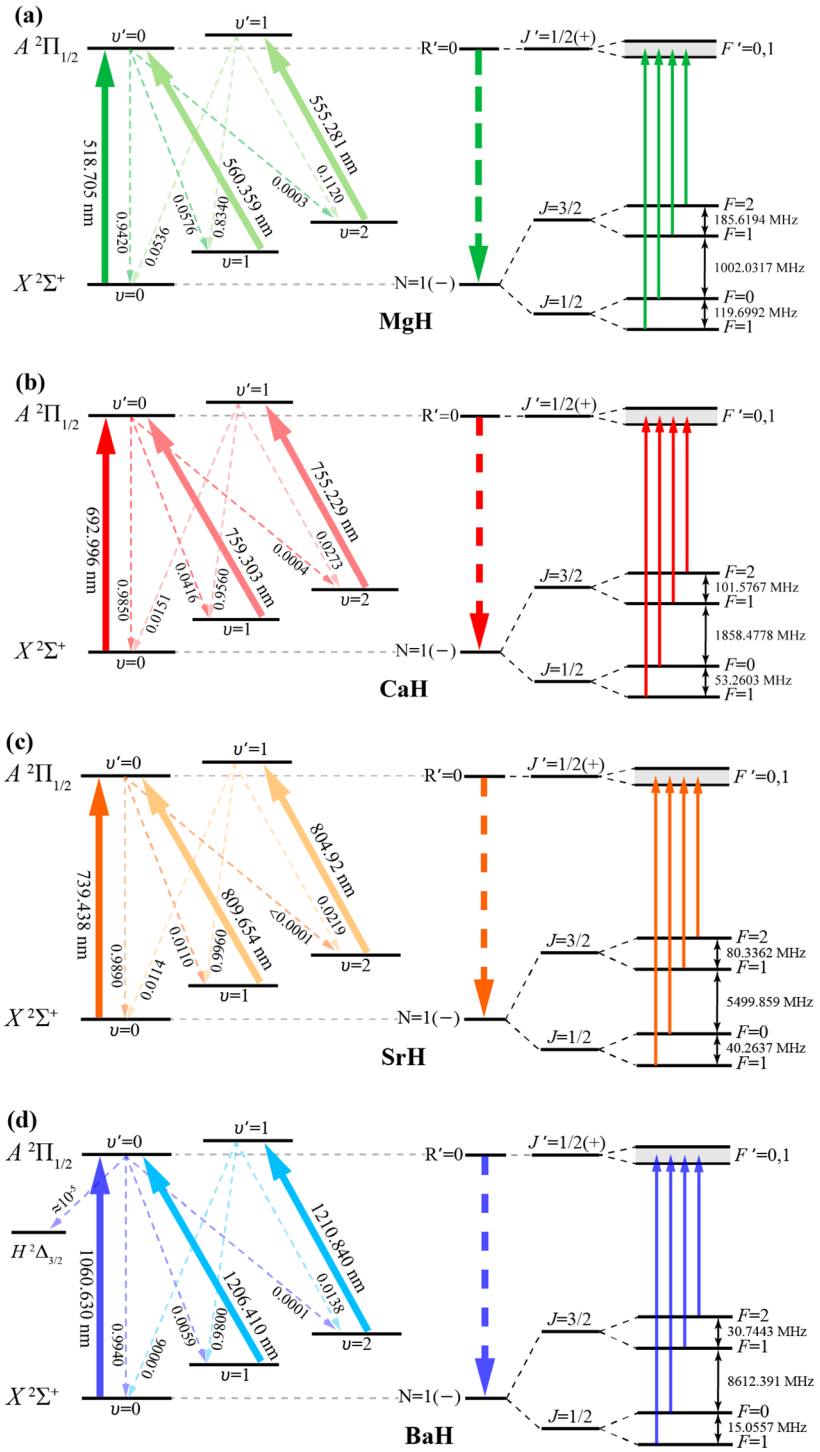

Figure 1. Vibrational level schemes of laser cooling (left column) and corresponding hyperfine manifolds (right column) for (a) MgH, (b) CaH, (c) SrH, and (d) BaH. Numbers along with thick solid lines indicate the pumping laser wavelenghs $\lambda_{vv'}$, while those along with thin dashed lines represent the FCFs $f_{v'v}$. Numbers beside double-arrows correspond to frequency intervals between two adjacent hyperfine levels. Thick dashed arrows indicate the spontaneous decay of $|A,v' = 0,J' = 1/2,+\rangle \rightarrow |X,v = 0,N = 1,-\rangle$.

https://doi.org/10.1021/acsomega.3c00352
ACS Omega 2023, 8, 19391−19401

Table 5. Comparison of the Calculated and Experimentally Measured Transition Frequencies for Hyperfine Translations in Rotational States of the $X^2\Sigma^+$ State of MgH, CaH, SrH, and BaH (Frequency Difference $\Delta\nu = \nu_{cal.} - \nu_{exp.}$ Is Defined)

Molecule	$N \rightarrow N'$	$J \rightarrow J'$	$F \rightarrow F'$	$\nu_{cal.}$ (MHz)	$\nu_{exp.}$ (MHz)	$\Delta\nu$ (kHz)
MgH	0 → 1	1/2 → 1/2	1 → 1	342997.7661	342997.763[72]	+3.1
			1 → 0	343117.4653	343117.463[72]	+2.3
			0 → 1	343305.6404	343305.646[72]	−5.6
		1/2 → 3/2	1 → 1	344119.4970	344119.497[72]	<0.1
			1 → 2	344305.1164	344305.125[72]	−8.6
			0 → 1	344427.3713	344427.362[72]	+9.3
CaH	0 → 1	1/2 → 1/2	1 → 1	252163.0907	252163.082[73]	+8.7
			1 → 0	252216.3510	252216.347[73]	+4.0
			0 → 1	252320.4557	252320.467[73]	−11.3
		1/2 → 3/2	1 → 1	254074.8288	254074.834[73]	−5.2
			1 → 2	254176.4055	254176.415[73]	−9.5
			0 → 1	254232.1938	254232.179[73]	+14.8
SrH	0 → 1	1/2 → 1/2	1 → 1	214229.4599	-	-
			1 → 0	214269.7236	-	-
			0 → 1	214351.1266	-	-
		1/2 → 3/2	1 → 1	219769.5824	-	-
			1 → 2	219849.9186	-	-
			0 → 1	219891.2491	-	-
BaH	0 → 1	1/2 → 1/2	1 → 1	195184.6383	-	-
			1 → 0	195199.6940	-	-
			0 → 1	195230.9716	-	-
		1/2 → 3/2	1 → 1	203812.0847	-	-
			1 → 2	203842.8290	-	-
			0 → 1	203858.4180	-	-

Besides the first excited state $A^2\Pi_{1/2}$, the second excited state $B^2\Sigma^+$ of some AEMHs may also be considered as the choice of the upper state for the optical cooling scheme.[53] Previously, Ramanaiah et al. had already calculated the FCFs from $B^2\Sigma^+(\upsilon' = 0)$ to $X^2\Sigma^+$ $(\upsilon = 0)$ of CaH and BaH, and both of them are highly diagonalized.[70] For the SrH molecule, the f_{00}, f_{01}, and f_{11} were computed as 0.9870, 0.0124, and 0.0005, respectively, by the RKR method, whose sum already reaches 0.9999. However, Moore and Lane have concluded that the $A^2\Pi_{1/2}$ state of BaH is a superior choice for the transition $B^2\Sigma^+(\upsilon' = 0)$ to $X^2\Sigma^+$ $(\upsilon = 0)$ having multiple tiny decay channels.[49] Besides, the FCFs between $B^2\Sigma^+(\upsilon' = 0)$ and $X^2\Sigma^+$ $(\upsilon = 2)$ are relatively small for MgH; thus, they are not suitable for the construction of a transition cycle.[71]

Hyperfine Structures and Transition Frequencies of the $X^2\Sigma^+$ State. In this section, we would like to calculate the hyperfine structures of the lowest rotational levels in the $X^2\Sigma^+$ state of AEMHs, which is insightful for implementing nearly closed optical transitions and the exploration of cold molecules at micro-Kelvin temperatures. We chose $A^2\Pi_{1/2} - X^2\Sigma^+$ as the cooling channel, wherein $X^2\Sigma^+$ is a Hund's case (b) state and $A^2\Pi_{1/2}$ is a Hund's case (a) state. Since N is a good quantum number for $X^2\Sigma^+$ but J is a good quantum number for $A^2\Pi_{1/2}$, we selected $|X,\upsilon = 0,N = 1,-\rangle$ as the ground state and $|A,\upsilon' = 0,J' = 1/2,+\rangle$ as the excited state in our study. Note that the nuclear spins of MH (^{24}MgH, ^{40}CaH, ^{88}SrH, and ^{138}BaH) are 0 for I_M and 1/2 for I_H respectively, leading to the total nuclear spin I of 1/2. Meanwhile, the total angular momentum $F = N + S + I$ indicating that the spin-rotational and hyperfine interactions can split the $|X,\upsilon = 0,N = 1,-\rangle$ state into four sublevels: $|J = 1/2,F = 0\rangle$, $|J = 1/2,F = 1\rangle$, $|J = 3/2,F = 1\rangle$ and $|J = 3/2,F = 2\rangle$. But for ^{9}BeH, the total nuclear spin can be 0 or 1 since $I_{Be} = 1/2$ and $I_H = 1/2$, and the energy level structure will be too complex to design the cooling scheme. Therefore, we only exclusively considered MH molecules (^{24}MgH, ^{40}CaH, ^{88}SrH, and ^{138}BaH) in the following calculations.

We adopted the effective Hamiltonian approach to evaluate the hyperfine structure in the $|X,\upsilon = 0,N = 1,-\rangle$ state of MgH, CaH, SrH, and BaH. For such a diatomic molecule in the Hund's case (b), the effective Hamiltonian contains the molecular rotational term H_R, the spin-rotational coupling H_{SR}, and the hyperfine interaction term H_{HFS}, and is given by

$$\begin{aligned} H_{\text{eff}} &= H_R + H_{SR} + H_{HFS} \\ H_R &= B_\upsilon \hat{N}^2 - D_\upsilon \hat{N}^4 \\ H_{SR} &= \gamma_\upsilon T^1(\hat{S}) T^1(\hat{N}) \\ H_{HFS} &= b_{F\upsilon} T^1(\hat{I}) T^1(\hat{S}) + c_\upsilon T^1_{q=0}(\hat{I}) T^1_{q=0}(\hat{S}) \\ &\quad + C_{\upsilon N} T^1(\hat{I}) T^1(\hat{N}) \end{aligned} \tag{1}$$

in which B_υ, D_υ, γ_υ, and $b_{F\upsilon}$ represent the rotational constant, the centrifugal distortion constant, the spin-rotational coupling constant, and the Fermi contact constant, respectively. In addition, $b_{F\upsilon} = b_\upsilon + c_\upsilon/3$, where b_υ and c_υ are connected with Frosch and Foley parameters. The nuclear spin-rotational constant $c_{\upsilon N}$, small enough compared with other constants, is neglected in our calculations. All required spectral constants are listed in Table 4.

The basis set in the Hund's case (b) coupling scheme can be represented as $|\phi\rangle = |\eta,N,S,J,I,F,M_F\rangle$, then we expressed the ground state matrix element of H_{eff} as

$$\begin{aligned} &\langle\phi'|B_\upsilon \hat{N}^2 - D_\upsilon \hat{N}^4|\phi\rangle \\ &= \delta_{N'N}\delta_{J'J}\delta_{F'F}\delta_{M'_F M_F} N(N+1)[B_\upsilon - D_\upsilon N(N+1)] \end{aligned} \tag{2}$$

https://doi.org/10.1021/acsomega.3c00352
ACS Omega 2023, 8, 19391−19401

Table 6. Computed Hyperfine Branching Ratios for the $|A,v' = 0,J' = 1/2,+\rangle \rightarrow |X,v = 0,N = 1,-\rangle$ transition of MgH, CaH, SrH, and BaH

				$F' = 0$	$F' = 1$							$F' = 0$	$F' = 1$		
Molecule	J	F	M_F	$M_{F'} = 0$	$M_{F'} = -1$	$M_{F'} = 0$	$M_{F'} = +1$	Molecule	J	F	M_F	$M_{F'} = 0$	$M_{F'} = -1$	$M_{F'} = 0$	$M_{F'} = +1$
MgH	3/2	2	−2	0	1/6	0	0	CaH	3/2	2	−2	0	1/6	0	0
			−1	0	1/12	1/12	0				−1	0	1/12	1/12	0
			0	0	1/36	1/9	1/36				0	0	1/36	1/9	1/36
			1	0	0	1/12	1/12				1	0	0	1/12	1/12
			2	0	0	0	1/6				2	0	0	0	1/6
		1	−1	0.0723	0.0515	0.0515	0			1	−1	0.0990	0.0342	0.0342	0
			0	0.0723	0.0515	0	0.0515				0	0.0990	0.0342	0	0.0342
			1	0.0723	0	0.0515	0.0515				1	0.0990	0	0.0342	0.0342
	1/2	1	−1	0.2610	0.1985	0.1985	0		1/2	1	−1	0.2343	0.2158	0.2158	0
			0	0.2610	0.1985	0	0.1985				0	0.2343	0.2158	0	0.2158
			1	0.2610	0	0.1985	0.1985				1	0.2343	0	0.2158	0.2158
		0	0	0	1/9	1/9	1/9			0	0	0	1/9	1/9	1/9
SrH	3/2	2	−2	0	1/6	0	0	BaH	3/2	2	−2	0	1/6	0	0
			−1	0	1/12	1/12	0				−1	0	1/12	1/12	0
			0	0	1/36	1/9	1/36				0	0	1/36	1/9	1/36
			1	0	0	1/12	1/12				1	0	0	1/12	1/12
			2	0	0	0	1/6				2	0	0	0	1/6
		1	−1	0.1079	0.0294	0.0294	0			1	−1	0.1103	0.0282	0.0282	0
			0	0.1079	0.0294	0	0.0294				0	0.1103	0.0282	0	0.0282
			1	0.1079	0	0.0294	0.0294				1	0.1103	0	0.0282	0.0282
	1/2	1	−1	0.2255	0.2206	0.2206	0		1/2	1	−1	0.2230	0.2218	0.2218	0
			0	0.2255	0.2206	0	0.2206				0	0.2230	0.2218	0	0.2218
			1	0.2255	0	0.2206	0.2206				1	0.2230	0	0.2218	0.2218
		0	0	0	1/9	1/9	1/9			0	0	0	1/9	1/9	1/9

$$\langle\phi'|\gamma_v T^1(\hat{S})T^1(\hat{N})|\phi\rangle = \delta_{N'N}\delta_{J'J}\delta_{F'F}\delta_{M'_F M_F}\gamma_v(-1)^{N+J+S} \times[S(S+1)(2S+1)]^{1/2}[N(N+1)(2N+1)]^{1/2} \times \begin{Bmatrix} S & N & J \\ N & S & 1 \end{Bmatrix} \quad (3)$$

$$\langle\phi'|b_v T^1(\hat{I})T^1(\hat{S})|\phi\rangle = \delta_{N'N}\delta_{F'F}\delta_{M'_F M_F}b_v(-1)^{J'+F+I+J+N+1+S} \times [(2J'+1)(2J+1)]^{1/2}[S(S+1)(2S+1)]^{1/2} \times [I(I+1)(2I+1)]^{1/2}\begin{Bmatrix} I & J' & F \\ J & I & 1 \end{Bmatrix}\begin{Bmatrix} J & S & N \\ S & J' & 1 \end{Bmatrix} \quad (4)$$

$$\langle\phi'|c_v T^1_{q=0}(\hat{I})T^1_{q=0}(\hat{S})|\phi\rangle = \delta_{N'N}\delta_{F'F}\delta_{M'_F M_F}\left(-\frac{\sqrt{30}}{3}\right)c_v(-1)^{J'+F+I+N} \times [(2J'+1)(2J+1)]^{1/2}[S(S+1)(2S+1)]^{1/2} \times [I(I+1)(2I+1)]^{1/2}(2N+1)\begin{pmatrix} N & 2 & N \\ 0 & 0 & 0 \end{pmatrix} \times \begin{Bmatrix} I & J' & F \\ J & I & 1 \end{Bmatrix}\begin{Bmatrix} J & J' & 1 \\ N & N & 2 \\ S & S & 1 \end{Bmatrix} \quad (5)$$

The corresponding eigenvalues and eigenvectors can be solved by the numerical diagonalization of the effective Hamiltonian matrix forms, and the energy splitting between two adjacent hyperfine levels and the closure of rotational structures are illustrated in Figure 1, in which the relevant FCFs and transition wavelengths are also indicated. The corresponding transition frequencies for all permitted hyperfine translations in rotational states of the $X^2\Sigma^+$ state of MH (M = Mg, Ca, Sr and Ba) are compiled in Table 5, which are well consistent with the data that obtained experimentally for MgH and CaH.[72,73] We have to mention that, though the leakage may occur between $R' = 0$ and $N = 3$ due to hyperfine structure mixing, the probability of such a leakage is very small. According to the second-order perturbation theory, the probability of leakage to the $X^2\Sigma^+(N = 3)$ state of these four molecules can be estimated to be less than 10^{-7}.[17,77]

Hyperfine Branching Ratios for the $A^2\Pi_{1/2} \leftarrow X^2\Sigma^+$ Transition. In this section, we calculated the hyperfine branching ratios for the $|A,v' = 0,J' = 1/2,+\rangle \leftarrow |X,v = 0,N = 1,-\rangle$ transition of MH (M = Mg, Ca, Sr, and Ba), which reflect the transition strengths determining the distribution of the laser intensity for all of the hyperfine decay paths. Prior to computing the branching ratios, J mixing in the $|X,v = 0,N = 1,-\rangle$ state from the superposition of pure J states has to be considered, which method was well described in ref 77. According to eqs 6.149 and 6.234 of ref 78, we can transform the basis set of the pure J state of $|X,N,J,F,-\rangle$ to the Hund's case (a) basis $|\Lambda,S,\Sigma,\Omega,J,I,F,M_F\rangle$ by eq 6, and $|A,J,+\rangle$ of Hund's case (a) can be expressed by eq 7. The electric dipole matrix elements were then calculated by eq 8, in which $T^1_p(\hat{d})$ is the electric dipole operator written in the spherical tensor. A similar method was also adopted in the cases of BaF[26] and MgF.[28] In Table 6, we list the hyperfine branching ratios for decays from hyperfine sublevels in $|A,J' = 1/2,+\rangle$ to hyperfine sublevels in $|X,N = 1,-\rangle$, and the sum of the branching ratios in each column reaches one as expected.

https://doi.org/10.1021/acsomega.3c00352
ACS Omega 2023, 8, 19391−19401

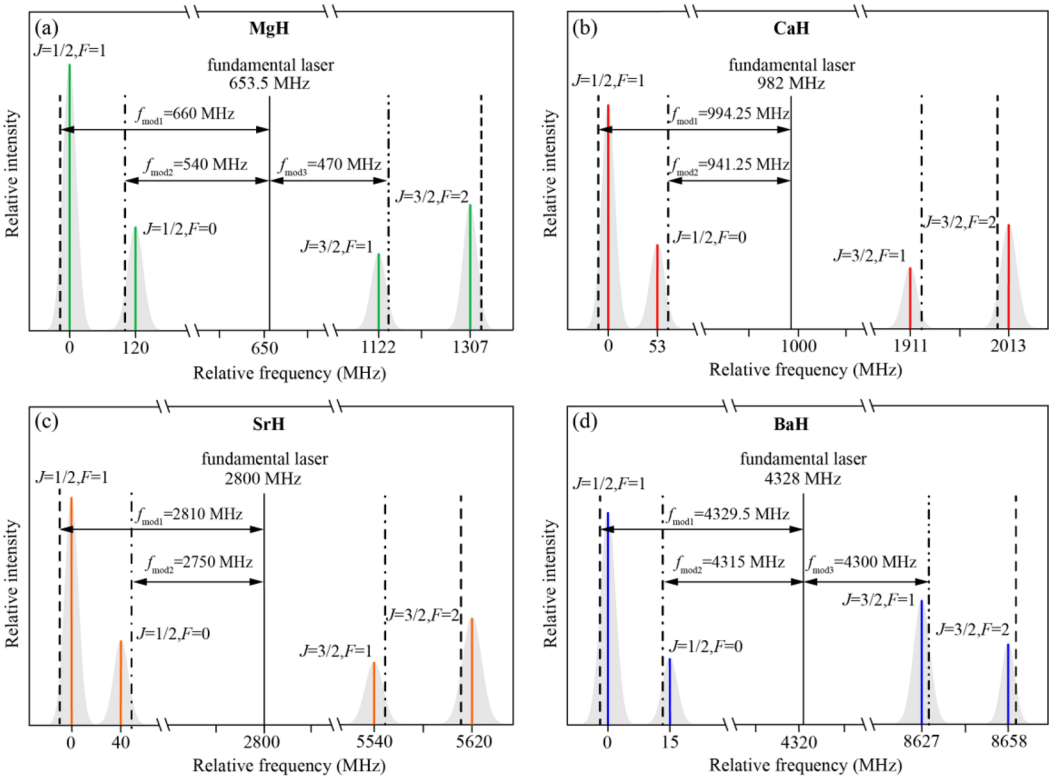

Figure 2. Sideband modulation for the hyperfine manifold of the ground state $|X,N = 1,-\rangle$ for (a) MgH, (b) CaH, (c) SrH, and (d) BaH, respectively. The fundamental frequency and the sideband positions for each molecule are indicated with respect to $|X,N = 1,J = 1/2,F = 1,-\rangle$, while colored solid lines mark the original frequencies of four hyperfine transition lines. Dashed, dash-dotted, and dot-dash-dotted black lines represent the modulating frequencies for the first, second, and third electro-optical modulators, respectively.

$$|\Lambda; N, S, J(F)\rangle = \sum_{\Omega}\sum_{\Sigma}(-1)^{J+\Omega}\sqrt{2N+1} \times \begin{pmatrix} S & N & F \\ \Sigma & \Lambda & -\Omega \end{pmatrix}|\Lambda; S, \Sigma; \Omega, J, F\rangle \tag{6}$$

$$|\Lambda^s, J, \pm\rangle = \frac{1}{\sqrt{2}}(|\Lambda^s; S, \Sigma; J, \Omega\rangle \pm (-1)^{J-S}|-\Lambda^s; S, -\Sigma; J, -\Omega\rangle) \tag{7}$$

$$\begin{aligned} m_{ij} &= \langle i|T_p^1(\hat{d})|j\rangle \\ &= \sum_{p=-1}^{1}(-1)^{F'-M_F'}\begin{pmatrix} F' & 1 & F \\ -M_F' & p & M_F \end{pmatrix}(-1)^{F+J'+I+1} \\ &\quad \times \sqrt{(2F'+1)(2F+1)}\begin{Bmatrix} J & F & I \\ F' & J' & 1 \end{Bmatrix} \\ &\quad \times \sum_{q=-1}^{1}(-1)^{J'-\Omega'}\begin{pmatrix} J' & 1 & J \\ -\Omega' & q & \Omega \end{pmatrix}\sqrt{(2J'+1)(2J+1)} \\ &\quad \times \langle \Lambda'; S, \Sigma'|T_q^1(d)|\Lambda; S, \Sigma\rangle \end{aligned} \tag{8}$$

Once the hyperfine structure and hyperfine branching ratios of the $|X,N = 1,-\rangle$ state are obtained, the sideband modulation scheme to simultaneously cover all hyperfine transitions can be proposed, which is shown in Figure 2. The fundamental laser frequency can be determined by the four hyperfine transitions originating from the $|X,N = 1,-\rangle$ state, leading to the minimum number of electro-optical modulators (EOMs) accounting for all of these hyperfine transitions, which is largely constrained by the principle hyperfine transition from $|X,N = 1,J = 1/2,F = 1,-\rangle$. To efficiently cover the hyperfine manifold, one has to consider the decay rate $\Gamma = 2\pi/\tau$ and the saturation irradiance $I_S = \pi hc\Gamma/(3\lambda^3)$ such that the detuning frequency within 3Γ with respect to each hyperfine peak might be practical in the sideband modulation (Table 7). Considering the economic costs and experimental complexity, at least two EOMs should be required to cover the hyperfine manifold of CaH and SrH, in contrast to three EOMs for MgH and BaH. Compared with AEMHs, the corresponding alkaline-earth-metal monofluorides (AEMFs) (*M*F, *M* = Mg, Ca, Sr, and Ba) have relatively shorter lifetimes (7.16, 19.2, 22.7, and 56 ns) and shorter wavelengths for the main cycling laser (359.3, 606, 663.3, and 859.8 nm), respectively.[11,13,26,28] Therefore, the saturation irradiance of these AEMFs can reach 62.7, 4.87, 3.14, and 0.58 mW/cm^2, respectively, indicating that these molecules requires much higher laser power in cooling and trapping than AEMHs. In addition, although the wavelengths for SrF and BaF are already accessible for diode lasers, those for MgF ($\lambda_{00} \approx 360$ nm) and CaF ($\lambda_{00} \approx 606$ nm) are still not readily available, so

Table 7. Decay Rates and Saturation Irradiance Values for *M*H (*M* = Mg, Ca, Sr, and Ba) Molecules

Molecules	λ_{00} (nm)	τ (ns)	$\Gamma/2\pi$ (MHz)	I_S (mW/cm^2)
MgH	518.705	43.6	3.650	3.421
CaH	692.996	33.2	4.794	1.884
SrH	739.438	33.8	4.709	1.523
BaH	1060.630	136.5	1.170	0.128

https://doi.org/10.1021/acsomega.3c00352
ACS Omega 2023, 8, 19391−19401

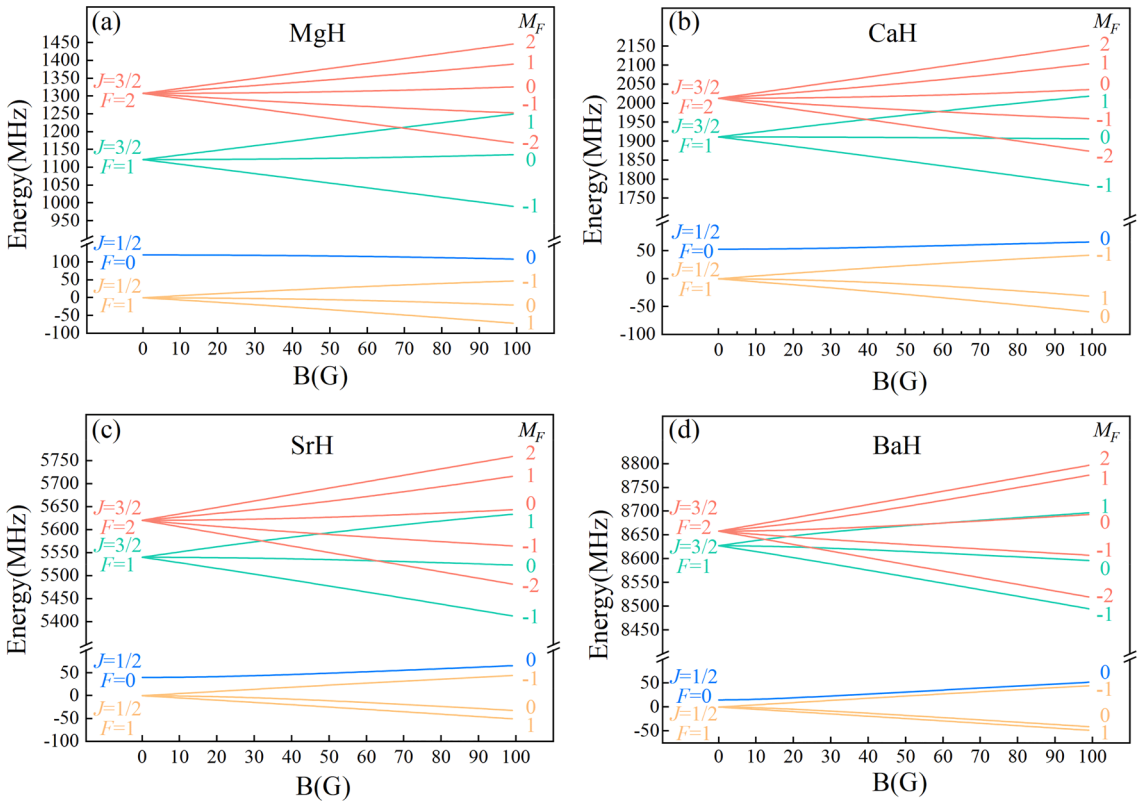

Figure 3. Zeeman energy level structures of the $|X,N = 1,-\rangle$ state for (a) MgH, (b) CaH, (c) SrH, and (d) BaH.

alternative high power lasers are considered for laser cooling such as the continuous tunable Ti:sapphire laser pumped by a solid state laser. Fortunately, CaH, SrH, and BaH require diode laser excitation wavelengths in the red or IR region, and laser diodes near 520 nm required for MgH have already become feasible in the past few years, thus making AEMHs relatively amenable to laser cooling using diode lasers.

Zeeman Structures for the $X^2\Sigma^+$ State. In this section, we analyzed the Zeeman interaction between the external magnetic field and the ground state hyperfine levels of *M*H (*M* = Mg, Ca, Sr, and Ba) molecules, in order to shed more light on the features of their magneto-optical trapping. Such a Zeeman interaction term is therefore added to the effective Hamiltonian in eq 1 to calculate the matrix elements, which can be expressed as

$$\hat{H}_{\text{Zeeman}} = g_s\mu_B T^1(\hat{S})T^1_{p=0}(\hat{B}) + g_L\mu_L T^1(\hat{L})T^1_{p=0}(\hat{B}) - g_I\mu_N T^1(\hat{I})T^1_{p=0}(\hat{B}) \quad (9)$$

Here, μ_B, μ_L, and μ_N represent the Bohr magneton, the magnetic moment arising from the electron orbital angular moment, and the nuclear magneton, while g_S, g_L, and g_I are the electron, electron orbital, and nuclear *g* factors, respectively. Considering that $\mu_B/\mu_N \approx 1836$ and $\Lambda = 0$, the term $g_s\mu_B T^1(\hat{S})T^1_{p=0}(\hat{B})$ in eq 9 is such a leading factor that the matrix expression of the Zeeman interaction can be simplified as

$$\begin{aligned}\langle\phi'|g_s\mu_B T^1(\hat{S})T^1_{p=0}(\hat{B})|\phi\rangle &= \delta_{N'N}\delta_{M_F,M_F'}g_s\mu_B B_Z(-1)^{F-M_F+F'+2J+I+N+S} \\ &\times [(2J+1)(2J'+1)(2F+1)(2F'+1)]^{1/2} \\ &\times [S(S+1)(2S+1)]^{1/2}\begin{Bmatrix} J & S & N \\ S & J' & 1 \end{Bmatrix} \\ &\times \begin{Bmatrix} F & J & I \\ J' & F' & 1 \end{Bmatrix}\begin{pmatrix} F & 1 & F' \\ -M_F & 0 & M_F \end{pmatrix}\end{aligned} \quad (10)$$

We present Zeeman structures of the $|X,N = 1,-\rangle$ state of *M*H molecules up to 100 G in Figure 3. In general, the magnetic sublevels of opposite M_F for the same *J* and *F* will split as the magnetic field grows but show linear dependence on the external magnetic field in the low field region. Since the typical magnetic field considered in a MOT experiment is about a few gauss, we further analyzed the *g* factors with and without *J* mixing by adopting $g_F = \Delta U/(M_F\mu_B B)$ in a small magnetic field according to the first-order perturbation theory, with ΔU being the corresponding energy difference (Table 8). For these molecules, both the $|J = 3/2,F = 2\rangle$ and $|J = 1/2,F = 0\rangle$ states have the same *g* factors that g_2 equals 0.5 and g_0 is close to zero with or without *J* mixing, in which the subscript numbers of the *g* factors indicate the *F* values. Meanwhile, for the $|J = 3/2,F = 1\rangle$ and $|J = 1/2,F = 1\rangle$ states, both g_1^+ and g_1^- with *J* mixing are getting closer to those without *J* mixing as the atomic number of the alkaline-earth metals increases, where superscripts "+" and "−" indicate $J = 3/2$ and 1/2 of $F = 1$, respectively.

https://doi.org/10.1021/acsomega.3c00352
ACS Omega 2023, 8, 19391−19401

Table 8. g Factors without and with J Mixing for the $|X,N = 1,-\rangle$ State of MgH, CaH, SrH, and BaH Molecules

		Molecule			
g factor	State label	MgH	CaH	SrH	BaH
Without J mixing	$\|J = 3/2,F = 2\rangle$	0.50	0.50	0.50	0.50
	$\|J = 3/2,F = 1\rangle$	0.83	0.83	0.83	0.83
	$\|J = 1/2,F = 1\rangle$	−0.33	−0.33	−0.33	−0.33
	$\|J = 1/2,F = 0\rangle$	0.00	0.00	0.00	0.00
With J mixing	$\|J = 3/2,F = 2\rangle$	0.50	0.50	0.50	0.50
	$\|J = 3/2,F = 1\rangle$	0.93	0.87	0.84	0.84
	$\|J = 1/2,F = 1\rangle$	−0.43	−0.37	−0.34	−0.34
	$\|J = 1/2,F = 0\rangle$	0.00	0.00	0.00	0.00

CONCLUSIONS

In conclusion, we have theoretically investigated the spectroscopic properties of alkaline-earth-metal monohydrides MH (M = Be, Mg, Ca, Sr, Ba) toward laser cooling and magneto-optical trapping. The highly diagonal Franck−Condon factors in the major cooling channel $X^2\Sigma^+ - A^2\Pi_{1/2}$ were first examined via the Morse potential method, the CFA method, and the RKR method, respectively, indicating that sum of f_{00}, f_{01}, and f_{02} for each molecule is greater than 0.9999 and almost 1×10^4 photons can be scattered to slow the molecules with only three lasers. The molecular hyperfine structures of the ground state $X^2\Sigma^+$, as well as hyperfine transitions and associated branching ratios in $A^2\Pi_{1/2}(J' = 1/2, +) \leftarrow X^2\Sigma^+$ ($N = 1,-$) of MgH, CaH, SrH, and BaH, are later evaluated via the effective Hamiltonian approach. These results not only confirm the consistency with the experimental hyperfine transitions of MgH and CaH but also provide the calculated hyperfine frequencies of the least explored SrH and BaH. Based on these, we proposed the sideband modulation schemes and found that at least two EOMs should be required for CaH and SrH, while three EOMs should be required for MgH and BaH, in order to implement the hyperfine transitions within 3Γ detuning. Lastly, we computed Zeeman energy level structures in the $|X,N = 1,-\rangle$ state and the associated magnetic g factors with or without J mixing in order to elucidate the magneto-optical trapping. Compared with the AEMFs (MF, M = Mg, Ca, Sr, Ba), the AEMHs show similar traits like the highly diagonal Franck−Condon factors, short lifetimes of the excited state, and no significant involvement of intervening electronic states. In addition, AEMHs require much less saturation irradiance than AEMFs and can benefit more from the diode lasers that are commercially available. Besides, Zelevinsky et al. have already calculated the realistic estimations of magneto-optical trapping forces for BaH molecules and the capture velocity in an AC configuration of a magneto-optical trap.[53] Further studies even revealed that heavier AEMH systems like SrH and BaH can have a fairly large permanent electric dipole moment, leading to impressive experimental sensitivity for precision measurement under long coherence time.[44] Therefore, our work outlined here would not only be beneficial to interpreting spectral data in astrophysics and helping design experimental systems related to laser cooling and magneto-optical trapping but also contribute to further studies about ultracold molecular collisions and exploration for fundamental physics beyond the standard model.

AUTHOR INFORMATION

Corresponding Authors

Jianping Yin − *State Key Laboratory of Precision Spectroscopy, East China Normal University, Shanghai 200062, P. R. China*; Email: jpyin@phy.ecnu.edu.cn

Tao Yang − *State Key Laboratory of Precision Spectroscopy, East China Normal University, Shanghai 200062, P. R. China; Collaborative Innovation Center of Extreme Optics, Shanxi University, Taiyuan, Shanxi 030006, P. R. China; Xinjiang Astronomical Observatory, Chinese Academy of Sciences, Urumqi, Xinjiang 830011, P. R. China;* orcid.org/0000-0003-4101-2385; Email: tyang@lps.ecnu.edu.cn

Authors

Renjun Pang − *State Key Laboratory of Precision Spectroscopy, East China Normal University, Shanghai 200062, P. R. China*

Junhao Yin − *State Key Laboratory of Precision Spectroscopy, East China Normal University, Shanghai 200062, P. R. China*

Yueyang Wang − *State Key Laboratory of Precision Spectroscopy, East China Normal University, Shanghai 200062, P. R. China*

Qinning Lin − *State Key Laboratory of Precision Spectroscopy, East China Normal University, Shanghai 200062, P. R. China*

Zesen Wang − *State Key Laboratory of Precision Spectroscopy, East China Normal University, Shanghai 200062, P. R. China*

Liang Xu − *Shanghai Key Laboratory of Modern Optical Systems, University of Shanghai for Science and Technology, Shanghai 200093, P. R. China*

Shunyong Hou − *State Key Laboratory of Precision Spectroscopy, East China Normal University, Shanghai 200062, P. R. China*

Hailing Wang − *State Key Laboratory of Precision Spectroscopy, East China Normal University, Shanghai 200062, P. R. China*

Complete contact information is available at: https://pubs.acs.org/10.1021/acsomega.3c00352

Notes

The authors declare no competing financial interest.

ACKNOWLEDGMENTS

Our work is supported by the National Natural Science Foundation of China (Grants Nos. 12274140 and 11874151), the Program for Professor of Special Appointment (Eastern Scholar) at Shanghai Institutions of Higher Learning, the Young Top-Notch Talent Support Program of Shanghai, and the Shanghai Natural Science Foundation (Grant No. 22ZR1421400).

REFERENCES

(1) Hudson, J. J.; Sauer, B. E.; Tarbutt, M. R.; Hinds, E. A. Measurement of the electron electric dipole moment using YbF molecules. *Phys. Rev. Lett.* **2002**, *89*, 023003.

(2) DeMille, D.; Cahn, S. B.; Murphree, D.; Rahmlow, D. A.; Kozlov, M. G. Using molecules to measure nuclear spin-dependent parity violation. *Phys. Rev. Lett.* **2008**, *100*, 023003.

https://doi.org/10.1021/acsomega.3c00352
ACS Omega 2023, 8, 19391−19401

(3) Murphy, M. T.; Flambaum, V. V.; Muller, S.; Henkel, C. Strong limit on a variable proton-to-electron mass ratio from molecules in the distant universe. *Science* **2008**, *320*, 1611.
(4) Zelevinsky, T.; Kotochigova, S.; Ye, J. Precision test of mass-ratio variations with lattice-confined ultracold molecules. *Phys. Rev. Lett.* **2008**, *100*, 043201.
(5) Chin, C.; Flambaum, V. V.; Kozlov, M. G. Ultracold molecules: new probes on the variation of fundamental constants. *New J. Phys.* **2009**, *11*, 055048.
(6) Kotochigova, S.; Zelevinsky, T.; Ye, J. Prospects for application of ultracold Sr_2 molecules in precision measurements. *Phys. Rev. A* **2009**, *79*, 012504.
(7) Baranov, M. A.; Dalmonte, M.; Pupillo, G.; Zoller, P. Condensed matter theory of dipolar quantum gases. *Chem. Rev.* **2012**, *112*, 5012.
(8) Cairncross, W. B.; Gresh, D. N.; Grau, M.; Cossel, K. C.; Roussy, T. S.; Ni, Y.; Zhou, Y.; Ye, J.; Cornell, E. A. Precision measurement of the electron's electric dipole moment using trapped molecular ions. *Phys. Rev. Lett.* **2017**, *119*, 153001.
(9) Bohn, J. L.; Rey, A. M.; Ye, J. Cold molecules: Progress in quantum engineering of chemistry and quantum matter. *Science* **2017**, *357*, 1002.
(10) Di Rosa, M. D. Laser-cooling molecules. *Eur. Phys. J. D* **2004**, *31*, 395.
(11) Shuman, E. S.; Barry, J. F.; Demille, D. Laser cooling of a diatomic molecule. *Nature* **2010**, *467*, 820.
(12) Barry, J. F.; McCarron, D. J.; Norrgard, E. B.; Steinecker, M. H.; DeMille, D. Magneto-optical trapping of a diatomic molecule. *Nature* **2014**, *512*, 286.
(13) Zhelyazkova, V.; Cournol, A.; Wall, T. E.; Matsushima, A.; Hudson, J. J.; Hinds, E. A.; Tarbutt, M. R.; Sauer, B. E. Laser cooling and slowing of CaF molecules. *Phys. Rev. A* **2014**, *89*, 053416.
(14) Hemmerling, B.; Chae, E.; Ravi, A.; Anderegg, L.; Drayna, G. K.; Hutzler, N. R.; Collopy, A. L.; Ye, J.; Ketterle, W.; Doyle, J. M. Laser slowing of CaF molecules to near the capture velocity of a molecular MOT. *J. Phys. B: At. Mol. Opt. Phys.* **2016**, *49*, 174001.
(15) Hummon, M. T.; Yeo, M.; Stuhl, B. K.; Collopy, A. L.; Xia, Y.; Ye, J. 2D Magneto-optical trapping of diatomic molecules. *Phys. Rev. Lett.* **2013**, *110*, 143001.
(16) Yeo, M.; Hummon, M. T.; Collopy, A. L.; Yan, B.; Hemmerling, B.; Chae, E.; Doyle, J. M.; Ye, J. Rotational state microwave mixing for laser cooling of complex diatomic molecules. *Phys. Rev. Lett.* **2015**, *114*, 223003.
(17) Shuman, E. S.; Barry, J. F.; Glenn, D. R.; DeMille, D. Radiative force from optical cycling on a diatomic molecule. *Phys. Rev. Lett.* **2009**, *103*, 223001.
(18) Barry, J. F.; Shuman, E. S.; Norrgard, E. B.; DeMille, D. Laser radiation pressure slowing of a molecular beam. *Phys. Rev. Lett.* **2012**, *108*, 103002.
(19) Steinecker, M. H.; McCarron, D. J.; Zhu, Y.; DeMille, D. Improved radio-frequency magneto-optical trap of SrF molecules. *ChemPhysChem* **2016**, *17*, 3664.
(20) Langin, T. K.; Jorapur, V.; Zhu, Y.; Wang, Q.; DeMille, D. Polarization enhanced deep optical dipole trapping of Λ-cooled polar molecules. *Phys. Rev. Lett.* **2021**, *127*, 163201.
(21) Truppe, S.; Williams, H. J.; Hambach, M.; Caldwell, L.; Fitch, N. J.; Hinds, E. A.; Sauer, B. E.; Tarbutt, M. R. Molecules cooled below the Doppler limit. *Nat. Phys.* **2017**, *13*, 1173.
(22) Anderegg, L.; Augenbraun, B. L.; Chae, E.; Hemmerling, B.; Hutzler, N. R.; Ravi, A.; Collopy, A.; Ye, J.; Ketterle, W.; Doyle, J. M. Radio frequency magneto-optical trapping of CaF with high density. *Phys. Rev. Lett.* **2017**, *119*, 103201.
(23) Collopy, A. L.; Ding, S.; Wu, Y.; Finneran, I. A.; Anderegg, L.; Augenbraun, B. L.; Doyle, J. M.; Ye, J. 3D Magneto-Optical Trap of Yttrium Monoxide. *Phys. Rev. Lett.* **2018**, *121*, 213201.
(24) Smallman, I. J.; Wang, F.; Steimle, T. C.; Tarbutt, M. R.; Hinds, E. A. Radiative branching ratios for excited states of ^{174}YbF: Application to laser cooling. *J. Mol. Spectrosc.* **2014**, *300*, 3.
(25) Isaev, T. A.; Hoekstra, S.; Berger, R. Laser-cooled RaF as a promising candidate to measure molecular parity violation. *Phys. Rev. A* **2010**, *82*, 052521.
(26) Chen, T.; Bu, W.; Yan, B. Structure, branching ratios, and a laser-cooling scheme for the ^{138}BaF molecule. *Phys. Rev. A* **2016**, *94*, 063415.
(27) Yang, Z. H.; Li, J.; Lin, Q. N.; Xu, L.; Wang, H. L.; Yang, T.; Yin, J. P. Laser-cooled HgF as a promising candidate to measure the electric dipole moment of the electron. *Phys. Rev. A* **2019**, *99*, 032502.
(28) Xu, L.; Yin, Y.; Wei, B.; Xia, Y.; Yin, J. Calculation of vibrational branching ratios and hyperfine structure of $^{24}Mg^{19}F$ and its suitability for laser cooling and magneto-optical trapping. *Phys. Rev. A* **2016**, *93*, 013408.
(29) Hendricks, R. J.; Holland, D. A.; Truppe, S.; Sauer, B. E.; Tarbutt, M. R. Vibrational branching ratios and hyperfine structure of ^{11}BH and its suitability for laser cooling. *Front. Phys.* **2014**, *2*, 51.
(30) Kozyryev, I.; Baum, L.; Matsuda, K.; Olson, P.; Hemmerling, B.; Doyle, J. M. Collisional relaxation of vibrational states of SrOH with He at 2 K. *New J. Phys.* **2015**, *17*, 045003.
(31) Kozyryev, I.; Baum, L.; Matsuda, K.; Augenbraun, B. L.; Anderegg, L.; Sedlack, A. P.; Doyle, J. M. Sisyphus laser cooling of a polyatomic molecule. *Phys. Rev. Lett.* **2017**, *118*, 173201.
(32) Kozyryev, I.; Hutzler, N. R. Precision measurement of time-reversal symmetry violation with laser-cooled polyatomic molecules. *Phys. Rev. Lett.* **2017**, *119*, 133002.
(33) Yadin, B.; Veness, T.; Conti, P.; Hill, C.; Yurchenko, S. N.; Tennyson, J. ExoMol line lists - I. The rovibrational spectrum of BeH, MgH and CaH in the $X^2\Sigma^+$ state. *Mon. Not. R. Astron. Soc.* **2012**, *425*, 34.
(34) Owens, A.; Dooley, S.; McLaughlin, L.; Tan, B.; Zhang, G.; Yurchenko, S. N.; Tennyson, J. ExoMol line lists - XLV. Rovibronic molecular line lists of calcium monohydride (CaH) and magnesium monohydride (MgH). *Mon. Not. R. Astron. Soc.* **2022**, *511*, 5448.
(35) Steimle, T. C.; Gengler, J.; Chen, J. A study of the $A^2\Pi/B^2\Sigma^+$-$X^2\Sigma^+$ band systems of calcium monohydride (CaH) using a supersonic molecular beam source and laser-induced fluorescence detection. *Can. J. Chem.* **2004**, *82*, 779.
(36) Appelblad, O.; Klynning, L.; Johns, J. W. C. Fourier transform spectroscopy of SrH: The A-X and B-X band systems. *Phys. Scr.* **1986**, *33*, 415.
(37) Hsiao, T.-C.; Luo, Y.-L.; Lin, K.-C.; Luh, W.-T. Laser spectroscopy on the MgH $A^2\Pi$-$X^2\Sigma^+$ band system. *J. Chin. Chem. Soc.* **1990**, *37*, 473.
(38) Focsa, C.; Firth, S.; Bernath, P. F.; Colin, R. Fourier transform emission spectroscopy of the $A^2\Pi$-$X^2\Sigma^+$ system of BeH. *J. Chem. Phys.* **1998**, *109*, 5795.
(39) Weinstein, J. D.; deCarvalho, R.; Guillet, T.; Friedrich, B.; Doyle, J. M. Magnetic trapping of calcium monohydride molecules at millikelvin temperatures. *Nature* **1998**, *395*, 148.
(40) Tscherbul, T. V.; Kłos, J.; Buchachenko, A. A. Ultracold spin-polarized mixtures of $^2\Sigma$ molecules with *S*-state atoms: Collisional stability and implications for sympathetic cooling. *Phys. Rev. A* **2011**, *84*, 040701.
(41) Singh, V.; Hardman, K. S.; Tariq, N.; Lu, M. J.; Ellis, A.; Morrison, M. J.; Weinstein, J. D. Chemical reactions of atomic lithium and molecular calcium monohydride at 1 K. *Phys. Rev. Lett.* **2012**, *108*, 203201.
(42) Gao, Y.; Gao, T. Laser cooling of the alkaline-earth-metal monohydrides: Insights from an *ab initio* theory study. *Phys. Rev. A* **2014**, *90*, 052506.
(43) El-Kork, N.; Zeid, I.; Al Razzouk, H.; Atwani, S.; Abou Arkoub, R.; Korek, M. Electronic structure with dipole moment calculations of the high-lying electronic states of BeH, MgH and SrH molecules. *J. Phys. Commun.* **2018**, *2*, 055030.
(44) Fazil, N. M.; Prasannaa, V. S.; Latha, K. V. P.; Abe, M.; Das, B. P. Electron correlation trends in the permanent electric dipole moments of alkaline-earth-metal monohydrides. *Phys. Rev. A* **2018**, *98*, 032511.

https://doi.org/10.1021/acsomega.3c00352
ACS Omega 2023, 8, 19391−19401

(45) Machado, F. B. C.; Roberto-Neto, O.; Ornellas, F. R. Radiative transition probabilities and lifetimes for the band systems $A^2\Pi$-$X^2\Sigma^+$ and $C^2\Sigma^+$-$X^2\Sigma^+$ of the BeH molecule. *Chem. Phys. Lett.* **1999**, *305*, 156.
(46) Nedelec, O.; Dufayard, J. Lifetimes of the MgH (MgD) and HgH (HgD) $A^2\Pi$ states excited by a pulsed dye laser. *J. Chem. Phys.* **1978**, *69*, 1833.
(47) Liu, M.; Pauchard, T.; Sjödin, M.; Launila, O.; van der Meulen, P.; Berg, L. E. Time-resolved study of the $A^2\Pi$ state of CaH by laser spectroscopy. *J. Mol. Spectrosc.* **2009**, *257*, 105.
(48) Berg, L. E.; Ekvall, K.; Hishikawa, A.; Kelly, S.; McGuinness, C. Laser spectroscopy of SrH. Time-resolved measurements of the $A^2\Pi$ state. *Chem. Phys. Lett.* **1996**, *255*, 419.
(49) Moore, K.; Lane, I. C. Quantitative theoretical analysis of lifetimes and decay rates relevant in laser cooling BaH. *J. Quant. Spectrosc. Radiat. Transfer* **2018**, *211*, 96.
(50) Moore, K.; Lane, I. C.; McNally, R. L.; Zelevinsky, T. Assignment of excited-state bond lengths using branching-ratio measurements: The $B^2\Sigma^+$ state of BaH molecules. *Phys. Rev. A* **2019**, *100*, 022506.
(51) Tarallo, M. G.; Iwata, G. Z.; Zelevinsky, T. BaH molecular spectroscopy with relevance to laser cooling. *Phys. Rev. A* **2016**, *93*, 032509.
(52) Iwata, G. Z.; McNally, R. L.; Zelevinsky, T. High-resolution optical spectroscopy with a buffer-gas-cooled beam of BaH molecules. *Phys. Rev. A* **2017**, *96*, 022509.
(53) McNally, R. L.; Kozyryev, I.; Vazquez-Carson, S.; Wenz, K.; Wang, T.; Zelevinsky, T. Optical cycling, radiative deflection and laser cooling of barium monohydride ($^{138}Ba^1H$). *New J. Phys.* **2020**, *22*, 083047.
(54) Yin, J.-H.; Yang, T.; Yin, J.-P. Theoretical investigation into spectrum of transition for CaH molecule toward laser cooling. *Acta Phys. Sin.* **2021**, *70*, 163302.
(55) Vázquez-Carson, S. F.; Sun, Q.; Dai, J.; Mitra, D.; Zelevinsky, T. Direct laser cooling of calcium monohydride molecules. *New J. Phys.* **2022**, *24*, 083006.
(56) Simon, P.; Moroshkin, P.; Weller, L.; Saß, A.; Weitz, M.; Seletskiy, D. V.; Sheik-Bahae, M. Towards redistribution laser cooling of molecular gases: production of candidtate molecules SrH by laser ablation. In *Laser Refrigeration of Solids VI*; Epstein, R. I., Seletskiy, D. E., Sheik-Bahae, M., Eds.; SPIE: 2013; Vol. *8638*; DOI: 10.1117/12.2002379.
(57) Berg, L.-E.; Klynning, L. Rotational analysis of the A-X and B-X band systems of CaH. *Phys. Scr.* **1974**, *10*, 331.
(58) *NIST Chemistry WebBook, NIST Standard Reference Database Number 69*; Linstrom, P. J., Mallard, W. G., Eds.; National Institute of Standards and Technology: Gaithersburg, MD, 2015; available at http://webbook.nist.gov.
(59) Shayesteh, A.; Appadoo, D. R.; Gordon, I.; Le Roy, R. J.; Bernath, P. F. Fourier transform infrared emission spectra of MgH and MgD. *J. Chem. Phys.* **2004**, *120*, 10002.
(60) Shayesteh, A.; Henderson, R. D.; Le Roy, R. J.; Bernath, P. F. Ground state potential energy curve and dissociation energy of MgH. *J. Phys. Chem. A* **2007**, *111*, 12495.
(61) Shayesteh, A.; Bernath, P. F. Rotational analysis and deperturbation of the $A^2\Pi$-$X^2\Sigma^+$ and $B'^2\Sigma^+$-$X^2\Sigma^+$ emission spectra of MgH. *J. Chem. Phys.* **2011**, *135*, 094308.
(62) Frank, A.; Rivera, A. L.; Wolf, K. B. Wigner function of Morse potential eigenstates. *Phys. Rev. A* **2000**, *61*, 054102.
(63) Nicholls, R. W. Franck-Condon factor formulae for astrophysical and other molecules. *Astrophys. J. Suppl. Ser.* **1981**, *47*, 279.
(64) Klein, O. Zur Berechnung von Potentialkurven fr zweiatomige Molekle mit Hilfe von Spektraltermen. *Z. Phys.* **1932**, *76*, 226.
(65) Rydberg, R. Graphische Darstellung einiger bandenspektroskopischer Ergebnisse. *Z. Phys.* **1932**, *73*, 376.
(66) Rydberg, R. Über einige Potentialkurven des Quecksilberhydrids. *Z. Phys.* **1933**, *80*, 514.
(67) Rees, A. L. G. The calculation of potential-energy curves from band-spectroscopic data. *Proc. Phys. Soc.* **1947**, *59*, 998.
(68) Spindler, R. J. Franck-Condon factors based on RKR potentials with applications to radiative absorption coefficients. *J. Quant. Spectrosc. Radiat. Transfer* **1965**, *5*, 165.
(69) Cheng, X.; Bai, J.; Yin, J. P.; Wang, H. L. Franck-Condon factors and band origins for MgH in the $A^2\Pi$-$X^2\Sigma^+$ system. *Chin. J. Chem. Phys.* **2015**, *28*, 253.
(70) Ramanaiah, M. V.; Lakshman, S. V. J. True potential energy curves and Franck-Condon factors of a few alkaline earth hydrides. *Phys. B+C* **1982**, *113*, 263.
(71) Mostafanejad, M.; Shayesteh, A. Ab initio potential energy curves and transition dipole moments for the $X^2\Sigma^+$, $A^2\Pi$ and $B'^2\Sigma^+$ states of MgH. *Chem. Phys. Lett.* **2012**, *551*, 13.
(72) Ziurys, L. M.; Barclay, W. L., Jr.; Anderson, M. A. The millimeter-wave spectrum of the MgH and MgD radicals. *Astrophys. J.* **1993**, *402*, L21.
(73) Barclay, W. L., Jr.; Anderson, M. A.; Ziurys, L. M. The millimeter-wave spectrum of CaH ($X^2\Sigma^+$). *Astrophys. J.* **1993**, *408*, L65.
(74) Shayesteh, A.; Walker, K. A.; Gordon, I.; Appadoo, D. R. T.; Bernath, P. F. New Fourier transform infrared emission spectra of CaH and SrH: combined isotopomer analyses with CaD and SrD. *J. Mol. Struct.* **2004**, *695*, 23−37.
(75) Weltner, W., Jr. *Magnetic Atoms and Molecules*; Van Nostrand: New York, 1983.
(76) Ram, R. S.; Bernath, P. F. Fourier transform emission spectroscopy of the $E^2\Pi$-$X^2\Sigma^+$ transition of BaH. *J. Mol. Spectrosc.* **2013**, *283*, 18.
(77) Sauer, B. E.; Wang, J.; Hinds, E. A. Laser-rf double resonance spectroscopy of ^{174}YbF in the $X^2\Sigma^+$ state: Spin-rotation, hyperfine interactions, and the electric dipole moment. *J. Chem. Phys.* **1996**, *105*, 7412.
(78) Brown, J. M.; Carrington, A. *Rotational Spectroscopy of Diatomic Molecules*; Cambridge University Press: Cambridge, 2003.

https://doi.org/10.1021/acsomega.3c00352
ACS Omega 2023, 8, 19391−19401